NEUTRON STARS: RECENT DEVELOPMENTS

HENNING HEISELBERG

Nordita, Blegdamsvej 17,
2100 Copenhagen Ø, Denmark
E-mail: hh@nordita.dk

Recent developments in neutron star theory and observation are discussed. Based on modern nucleon-nucleon potentials more reliable equations of state for dense nuclear matter have been constructed. Furthermore, phase transitions such as pion, kaon and hyperon condensation, superfluidity and quark matter can occur in cores of neutron stars. Specifically, the nuclear to quark matter phase transition and its mixed phases with intriguing structures is treated. Rotating neutron stars with and without phase transitions are discussed and compared to observed masses, radii and glitches. The observations of possible heavy $\sim 2M_\odot$ neutron stars in X-ray binaries and QPO's require relatively stiff equation of states and restrict strong phase transitions to occur at very high nuclear densities only.

1 Introduction

Neutron stars are complicated many-body systems of neutrons, protons, electrons and muons with possibly additional intricate phases of pion, kaon, hyperon or quark condensates. It is therefore appropriate that neutron stars are included at this "Xth Intl. Conf. on Recent Progress in Many-body Theories".

A brief history of the most important discoveries in this millennium concerning neutron stars listed in Table I. Most are well known except perhaps for the most recent ones discussed the following sections: Sec. 2 list neutron star masses from binary pulsars and X-ray binaries and specifically discuss recent masses and radii from quasi periodic oscillations in low mass X-ray pulsars. In Sec. 3 we turn to modern equation of states for neutron star matter with particular attention to the uncertainty in the stiffness of the equation of state at high densities and causality constraints. Sec. 4 attempts to give an up-to-date on possible phase transitions to kaon and pion condensates, hyperon and quark matter, superfluidity, etc. Sec. 5 contains the resulting structure of neutron stars, calculated masses and radii, and compares to observations. In Sec. 6 observational effects of glitches are described when phase transitions occur. Sec. 7 contain novel information on connections between supernova remnants and NO_3^- peaks in ice cores, X-ray bursts and thermonuclear explosions, gamma ray bursters and neutron star collapse to black holes. Finally, a summary and conclusion is given. For more details we refer to [1].

2 Observed neutron star masses and QPO's

The best determined neutron star masses are found in binary pulsars and all lie in the range $1.35 \pm 0.04 M_\odot$ [2]. These masses have been accurately determined from variations in their radio pulses due to doppler shifts as well periastron advances of

Table 1: Chronological list of important developments related to neutron stars

Year	"Observers"	Discovery
1054	Chinese	record the Crab Supernova
1572	Tycho Brahe	observes a Supernova
1932	Chadwick	discovers the neutron
1932	Landau & others	suggests the existence of neutron stars
1934	Baade & Zwicky	connects supernovae to gravitational collapse of stars to neutron stars
1935	Oppenheimer & Volkoff	calculate first neutron star structures
1946	Gamow	develops nucleosynthesis which requires heavier elements from Supernovae
1967	Bell & Hewish	discover first pulsar
1969		pulsars in Crab and Vela Supernova remnants
1973	Hulse & Taylor	discover first binary pulsar
1987	Neutrino detectors	collect 19 neutrinos from SN-1987A
1995	Nijmegen data base	compilation of $\gtrsim$5000 NN cross sections leads to "modern" NN potentials and EoS
1996	RXTE	kHz oscillations (QPO) in X-ray binaries
1997	BeppoSAX	Gamma Ray Burst with afterglow at $z\gtrsim 1$ Beaming and syncroton radiation observed
1998	Supernova remnants	match dating of polar ice core NO_3^--peaks

their close elliptic orbits that are strongly affected by general relativistic effects. One exception is the nonrelativistic pulsar PSR J1012+5307 of mass[a] $M = (2.1 \pm 0.8) M_\odot$ [3].

Several X-ray binary masses have been measured of which the heaviest are Vela X-1 with[4] $M = (1.9 \pm 0.2) M_\odot$ and Cygnus X-2 with[5] $M = (1.8 \pm 0.4) M_\odot$. Their Kepler orbits are determined by measuring doppler shift of both the X-ray binary and its companion. To complete the mass determination one needs the orbital inclination which is determined by eclipse durations, optical light curves, or polarization variations[3].

The recent discovery of high-frequency brightness oscillations in low-mass X-ray binaries provides a promising new method for determining masses and radii of neutron stars[6]. The kilohertz quasi-periodic oscillations (QPO) occur in pairs and are most likely the orbital frequencies

$$\nu_{QPO} = (1/2\pi)\sqrt{GM/R^3_{orb}}\,, \tag{1}$$

of accreting matter in Keplerian orbits around neutron stars of mass M and its beat frequency with the neutron star spin, $\nu_{QPO} - \nu_s$. The accretion can for a few QPO's be tracked to its innermost stable orbit [7,8]

$$R_{ms} = 6GM/c^2\,. \tag{2}$$

[a] All uncertainties given here are 95% conf. limits or $\sim 2\sigma$

For slowly rotating stars the resulting mass is from Eqs. (1,2)

$$M \simeq 2.2 M_\odot \frac{\mathrm{kHz}}{\nu_{QPO}} \,. \tag{3}$$

For example, the maximum frequency of 1060 Hz upper QPO observed in 4U 1820-30 gives $M \simeq 2.25 M_\odot$ after correcting for the $\nu_s \simeq 275$ Hz neutron star rotation frequency. If the maximum QPO frequencies of 4U 1608-52 ($\nu_{QPO} = 1125$ Hz) and 4U 1636-536 ($\nu_{QPO} = 1228$ Hz) also correspond to innermost stable orbits the corresponding masses are $2.1 M_\odot$ and $1.9 M_\odot$. Evidence for the innermost stable orbit has been found for 4U 1820-30, where ν_{QPO} display a distinct saturation with accretion rate indicating that orbital frequency cannot exceed that of the innermost stable orbit. However, one caveat is that large accretion leads to radiation that can slow down the rotation of the accreting matter. More observations are needed before a firm conclusion can be made.

Large neutron star masses of order $\sim 2 M_\odot$ would restrict the equation of state (EoS) severely for dense matter as addressed in the following.

3 Modern nuclear equation of states

Recent models for the nucleon-nucleon (NN) interaction, based on the compilation of more than 5000 NN cross sections in the Nijmegen data bank, have reduced the uncertainty in NN potentials. The last Indiana run at higher momenta will further reduce uncertainties in NN interactions. Including many-body effects, three-body forces, relativistic effects, etc., the nuclear EoS have been constructed with reduced uncertainty allowing for more reliable calculations of neutron star properties [10]. Likewise, recent realistic effective interactions for nuclear matter obeying causality at high densities, constrain the EoS severely and thus also the maximum masses of neutron stars. We have in [1] elaborated on these analyses by incorporating causality smoothly in the EoS for nuclear matter allowing for first and second order phase transitions to, e.g., quark matter.

For the discussion of the gross properties of neutron stars we will use the optimal EoS of Akmal, Pandharipande, & Ravenhall [10] (specifically the Argonne $V18 + \delta v +$ UIX* model- hereafter APR98), which is based on the most recent models for the nucleon-nucleon interaction, see Engvik et al. [12] for a discussion of these models, and with the inclusion of a parametrized three-body force and relativistic boost corrections. The EoS for nuclear matter is thus known to some accuracy for densities up to a few times nuclear saturation density $n_0 = 0.16$ fm^{-3}. We parametrize the APR98 EoS by a simple form for the compressional and symmetry energies that gives a good fit around nuclear saturation densities and smoothly incorporates causality at high densities such that the sound speed approaches the speed of light. This requires that the compressional part of the energy per nucleon is quadratic in nuclear density with a minimum at saturation but linear at high densities

$$\begin{aligned} \mathcal{E} &= E_{comp}(n) + S(n)(1-2x)^2 \\ &= \mathcal{E}_0 u \frac{u-2-s}{1+su} + S_0 u^\gamma (1-2x)^2. \end{aligned} \tag{4}$$

Here, $n = n_p + n_n$ is the total baryon density, $x = n_p/n$ the proton fraction and $u = n/n_0$ is the ratio of the baryon density to nuclear saturation density. The compressional term is in Eq. (4) parametrized by a simple form which reproduces the saturation density and the binding energy per nucleon $\mathcal{E}_0 = 15.8$MeV at n_0 of APR98. The "softness" parameter $s \simeq 0.2$, which gave the best fit to the data of APR98 is determined [1] by fitting the energy per nucleon of APR98 up to densities of $n \sim 4n_0$. For the symmetry energy term we obtain $S_0 = 32$ MeV and $\gamma = 0.6$ for the best fit. The proton fraction is given by β-equilibrium at a given density.

The one unknown parameter s expresses the uncertainty in the EoS at high density and we shall vary this parameter within the allowed limits in the following with and without phase transitions to calculate mass, radius and density relations for neutron stars. The "softness" parameter s is related to the incompressibility of nuclear matter as $K_0 = 18\mathcal{E}_0/(1+s) \simeq 200$MeV. It agrees with the poorly known experimental value [26], $K_0 \simeq 180 - 250$MeV which does not restrict it very well. From $(v_s/c)^2 = \partial P/\partial(n\mathcal{E})$, where P is the pressure, and the EoS of Eq. (4), the causality condition $c_s \leq c$ requires

$$s \gtrsim \sqrt{\frac{\mathcal{E}_0}{m_n}} \simeq 0.13\,, \tag{5}$$

where m_n is the mass of the nucleon. With this condition we have a causal EoS that reproduces the data of APR98 at densities up to $0.6 \sim 0.7$ fm^{-3}. In contrast, the EoS of APR98 becomes superluminal at $n \approx 1.1$ fm^{-3}. For larger s values the EoS is softer which eventually leads to smaller maximum masses of neutron stars. The observed $M \simeq 1.4M_\odot$ in binary pulsars restricts s to be less than $0.4 - 0.5$ depending on rotation as shown in calculations of neutron stars below.

In Fig. 1 we plot the sound speed $(v_s/c)^2$ for various values of s and that resulting from the microscopic calculation of APR98 for β-stable pn-matter. The form of Eq. (4), with the inclusion of the parameter s, provides a smooth extrapolation from small to large densities such that the sound speed v_s approaches the speed of light. For $s = 0.0$ ($s = 0.1$) the EoS becomes superluminal at densities of the order of 1 (6) fm^{-3}.

The sound speed of Kalogera & Baym [11] is also plotted in Fig. 1. It jumps discontinuously to the speed of light at a chosen density. With this prescription they were able to obtain an optimum upper bound for neutron star masses and obey causality. This prescription was also employed by APR98. The EoS is thus discontinuously stiffened by taking $v_s = c$ at densities above a certain value n_c which, however, is lower than $n_s = 5n_0$ where their nuclear EoS becomes superluminal. This approach stiffens the nuclear EoS for densities $n_c < n < n_s$ but softens it at higher densities. Their resulting maximum masses lie in the range $2.2M_\odot \lesssim M \lesssim 2.9M_\odot$. Our approach however, incorporates causality by reducing the sound speed smoothly towards the speed of light at high densities. Therefore our approach will not yield an absolute upper bound on the maximum mass of a neutron star but gives reasonable estimates based on modern EoS around nuclear matter densities, causality constraints at high densities and a smooth extrapolation between these two limits (see Fig. 1).

At very high densities particles are expected to be relativistic and the sound

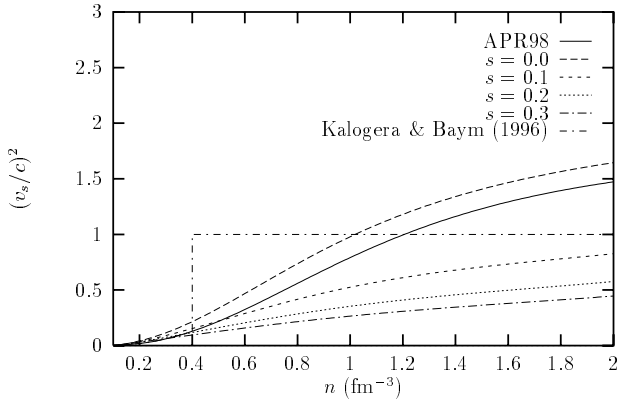

Figure 1: $(v_s/c)^2$ for β-stable pn-matter for $s = 0, 0.1, 0.2, 0.3$, the results of APR98, and for the patched EoS of Kalogera & Baym which shows a discontinuous $(v_s/c)^2$.

speed should be smaller than the speed of light, $v_s^2 \simeq c^2/3$. Consequently, the EoS should be even softer at high densities and the maximum masses we obtain with the EoS of (4) are likely to be too high estimates.

4 Phase transitions

The physical state of matter in the interiors of neutron stars at densities above a few times normal nuclear matter densities is essentially unknown and many first and second order phase transitions have been speculated upon.

4.1 Kaon condensation

Kaon condensation in dense matter was suggested by Kaplan and Nelson [13], and has been discussed in many recent publications [14,15]. Due to the attraction between K^- and nucleons its energy decreases with increasing density, and eventually if it drops below the electron chemical potential in neutron star matter in β-equilibrium, a Bose condensate of K^- will appear. It is found that K^-'s condense at densities above $\sim 3 - 4\rho_0$, where $\rho_0 = 0.16$ fm^{-3} is normal nuclear matter density. This is to be compared to the central density of $\sim 4\rho_0$ for a neutron star of mass $1.4M_\odot$ according to the estimates of Wiringa, Fiks and Fabrocini [16] using realistic models of nuclear forces.

In neutron matter at low densities, when the interparticle spacing is much larger than the range of the interaction, $r_0 \gg R$, the kaon interacts strongly many times with the same nucleon before it encounters and interacts with another nucleon. Thus one can use the scattering length as the "effective" kaon-neutron interaction,

$a_{K^-N} \simeq -0.41$fm, where we ignore the minor proton fraction in nuclear matter. The kaon energy deviates from its rest mass by the Lenz potential

$$\omega_{Lenz} = m_K + \frac{2\pi}{m_R}\, a_{K^-N}\, n_{NM}, \tag{6}$$

which is the optical potential obtained in the impulse approximation. If hadron masses furthermore decrease with density the condensation will occur at lower densities [14].

At high densities when the interparticle spacing is much less than the range of the interaction, $r_0 \ll R$, the kaon will interact with many nucleons on a distance scale much less than the range of the interaction. The kaon thus experiences the field from many nucleons and the kaon energy deviates from its rest mass by the Hartree potential:

$$\omega_{Hartree} = m_K + n_{NM} \int V_{K^-N}(r) d^3r\,, \tag{7}$$

As shown in Ref. [17], the Hartree potential is considerably less attractive than the Lenz potential. Already at rather low densities, when the interparticle distance is comparable to the range of the KN interaction, the kaon-nucleon and nucleon-nucleon correlations conspire to reduce the K^-N attraction significantly [17,18]. This is also evident from Fig. 2 where the transition from the low density Lenz potential to the high density Hartree potential is calculated by solving the Klein-Gordon equation for kaons in neutron matter in the Wigner-Seitz cell approximation. Results are for square well K^-N-potentials of various ranges R. For the measured K^-n scattering lengths and reasonable ranges of interactions the attraction is reduced by about a factor of 2-3 in cores of neutron stars. Relativistic effects further reduce the attraction at high densities. Consequently, a kaon condensate is less likely in neutron stars due to nuclear correlations.

If the kaon condensate occurs a mixed phase of kaon condensates and ordinary nuclear matter may coexist in a mixed phase [19] depending on surface and Coulomb energies involved. The structures would be much like the quark and nuclear matter mixed phases described above.

4.2 Pion condensation

Pion condensation is like kaon condensation possible in dense neutron star matter (see, e.g., [20,21]). If we first neglect the effect of strong correlations of pions with the matter in modifying the pion self-energy, one finds it is favorable for a neutron on the top of the Fermi sea to turn into a proton and a π^- when

$$\mu_n - \mu_p = \mu_e > m_{\pi^-}, \tag{8}$$

where $m_{\pi^-} = 139.6$ MeV is the π^- rest mass. As discussed in the previous subsection, at nuclear matter saturation density the electron chemical potential is ~ 100 MeV and one might therefore expect the appearance of π^- at a slightly higher density. One can however not neglect the interaction of the pion with the background

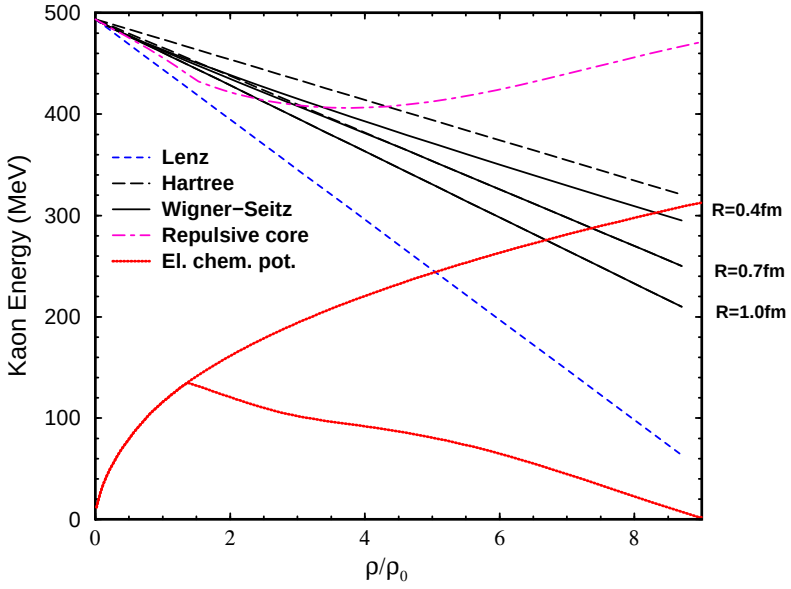

Figure 2: Kaon energy as function of neutron density is shown by full curves for various ranges of the K^-n potentials $R = 0.4, 0.7, 1.0$ fm. Nuclear correlations change the low density Lenz result (Eq. (6), dotted curve) to the high density Hartree result (Eq.(7), dashed curves). The electron chemical potential μ_e from the EoS of Eq. (4) with $\delta = 0.2$ is shown with and without (lower and upper dotted curves) a transition to a mixed phase of quark matter for $B = 100$ MeVfm^{-3}.

matter. Such interactions can enhance the pion self-energy and thereby the pion threshold density, and depending on the chosen parameters, see again Ref. [21], the critical density for pion condensation may vary from n_0 to $4n_0$. These matters are however not yet settled in a satisfying way, and models with strong nucleon-nucleon correlations tend to suppress both the πNN and $\pi\Delta N$ interaction vertices so that a pion condensation in neutron star matter does not occur.

A π^0 condensate may also form as recently suggested by Akmal et al. [10] and appears at a density of ~ 0.2 fm^{-3} for pure neutron matter when the three-body interaction is included, whereas without V_{ijk} it appears at much higher densities, i.e. ~ 0.5 fm^{-3}. The π^0 are virtual in the same way as the photons keeping a solid together are virtual.

4.3 Hyperon matter

Condensates of hyperons $\Lambda, \Sigma^{-,0,+}, ...$ and Deltas $\Delta^{-,0,+,++}$ also appear when their chemical potential exceeds their effective mass in matter. In β-equilibrium the chemical potentials are related by

$$\mu_n + \mu_e = \mu_{\Sigma^-} = \mu_{\Delta^-} \tag{9}$$

$$\mu_n = \mu_\Lambda = \mu_{\Sigma^0} = \mu_{\Delta^0} \tag{10}$$

$$\mu_p = \mu_{\Delta^+} \, . \tag{11}$$

The Σ^- appears via weak strangeness non-conserving interactions $e^- + n \to \Sigma^- + \nu_e$, when $\mu_{\Sigma^-} > \omega_{\Sigma^-}$ and Λ hyperons when $\mu_\Lambda > \omega_\Lambda$ If we neglect interactions, one would expect the Σ^- to appear at lower densities than the Λ, even though Σ^- is more massive due to the large electron chemical potential. The threshold densities for noninteracting $\Sigma^-, \Delta^-, \Lambda$ are relatively low indicating that these condensates are present in cores of neutron stars if their interactions can be ignored.

Hyperon energies are, however, strongly affected in dense nuclear matter by interactions and correlations with the nucleons and other hyperons in a condensate. If hyperons have the short range repulsion and three-body interactions as nucleons, a condensate of hyperons become less likely.

4.4 Quark matter

Eventually at high densities, we expect hadrons to deconfine to quark matter or, in other words, chiral symmetry to be restored. This transition has been extensively studied by the Bag model equation of state (EoS) for quark matter which leads to a first order phase transition from hadronic to quark matter at a density and temperature determined by the parameters going into both EoS. In the bag model the quarks are assumed to be confined to a finite region of space, the so-called 'bag', by a vacuum pressure B. Adding the Fermi pressure and interactions computed to order $\alpha_s = g^2/4\pi$, where g is the QCD coupling constant, the total pressure for three massless quarks of flavor $f = u, d, s$, is

$$P = \frac{3\mu_f^4}{4\pi^2}(1 - \frac{2}{\pi}\alpha_s) - B + P_e + P_\mu \,, \tag{12}$$

where $P_{e,\mu}$ are the electron and muon pressure, e.g., $P_e = \mu_e^4/12\pi^2$. A Fermi gas of quarks of flavor i has density $n_i = k_{Fi}^3/\pi^2$, due to the three color states. A finite strange quark mass have minor effect on the EoS since quark chemical potentials $\mu_q \gtrsim m_N/3$ typically are much larger. The value of the bag constant B is poorly known, and we present results using two representative values, $B = 150$ MeVfm^{-3} and $B = 200$ MeVfm^{-3}. We take $\alpha_s = 0.4$. However, similar results can be obtained with smaller α_s and larger B.

The quark and nuclear matter mixed phase has continuous pressures and densities due to the general Gibbs criteria for two-component systems [27]. There are no first order phase transitions but at most two second order phase transitions. Namely, at a lower density, where quark matter first appears in nuclear matter, and at a very high density (if gravitationally stable), where all nucleons are finally dissolved into quark matter. This mixed phase does, however, not include local surface and Coulomb energies of the quark and nuclear matter structures. If the interface tension between quark and nuclear matter is too large, the mixed phase is not favored energetically due to surface and Coulomb energies associated with forming these structures [28]. The neutron star will then have a core of pure quark matter with a mantle of nuclear matter surrounding it and the two phases are co-existing by a first order phase transition or Maxwell construction. For a small or moderate interface tension the quarks are confined in droplet, rod- and plate-like structures as found in the inner crust of neutron stars (see [23] and Fig. 3).

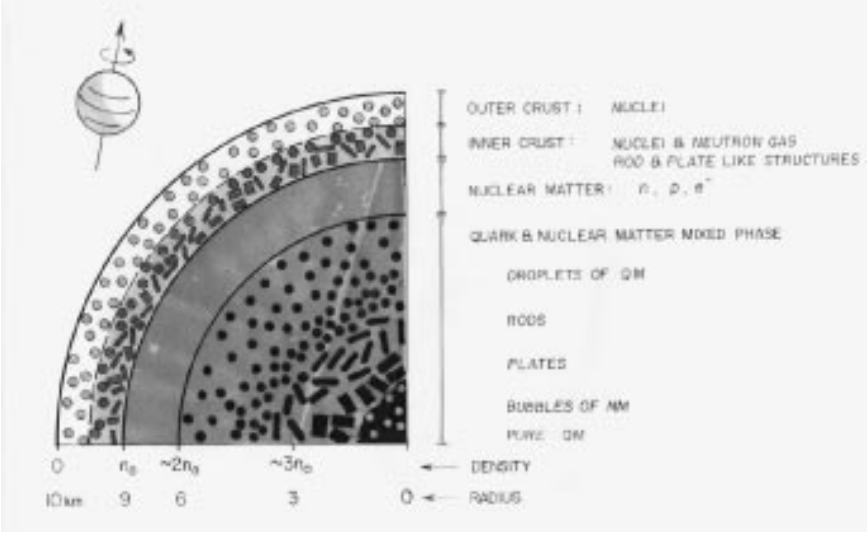

Figure 3: The quark and nuclear matter structure in a quarter of a typical $1.4 M_\odot$ solar mass neutron star. The typical sizes of structures are a few Fermi's but have been scaled up by about 16 orders of magnitudes to be seen.

4.5 Superfluidity in baryonic matter

The presence of neutron superfluidity in the crust and the inner part of neutron stars are considered well established in the physics of these compact stellar objects. In the low density outer part of a neutron star, the neutron superfluidity is expected mainly in the attractive $^1S_0$ channel. At higher density, the nuclei in the crust dissolve, and one expects a region consisting of a quantum liquid of neutrons and protons in beta equilibrium. The proton contaminant should be superfluid in the $^1S_0$ channel, while neutron superfluidity is expected to occur mainly in the coupled $^3P_2$-$^3F_2$ two-neutron channel. In the core of the star any superfluid phase should finally disappear.

Dilute Fermi systems can now be studied as atomic gases recently have been cooled down to nanokelvin similar to Bose-Einstein condensates. Degeneracy was observed [24] and BCS gaps are currently searched for. According to Gorkov and Melik-Bharkuderov [25] the gap is

$$\Delta = \left(\frac{2}{e}\right)^{7/3} \frac{k_F^2}{2m} \exp\left[\frac{\pi}{2ak_F}\right] \tag{13}$$

in the dilute limit where the Fermi momentum times the scattering length is small, $k_F|a| \ll 1$.

Recently color superconductivity in quark matter has been taken up again since the quark color interaction has been conjectured to be large. Correspondingly large gaps of order tens of MeV are found. If the strange quark mass is sufficiently small color-flavor locking occur between up and down or strange quarks. We refer to T. Schaefer these proceedings for further details.

5 Calculated neutron star masses and radii

In order to obtain the mass and radius of a neutron star, we have solved the Tolman-Oppenheimer-Volkov equation with and without rotational corrections. The equations of state employed are given by the *pn*-matter EoS with $s = 0.13, 0.2, 0.3, 0.4$ with nucleonic degrees of freedom only. In addition we have selected two representative values for the bag-model parameter B, namely 150 and 200 MeVfm^{-3} for our discussion on eventual phase transitions. The quark phase is linked with our *pn*-matter EoS from Eq. (4) with $s = 0.2$ through either a mixed phase construction or a Maxwell construction [1]. For $B = 150$ MeVfm^{-3}, the mixed phase begins at 0.51 fm^{-3} and the pure quark matter phase begins at 1.89 fm^{-3}. Finally, for $B = 200$ MeVfm^{-3}, the mixed phase starts at 0.72 fm^{-3} while the pure quark phase starts at 2.11 fm^{-3}. In case of a Maxwell construction, in order to link the *pn* and the quark matter EoS, we obtain for $B = 150$ MeVfm^{-3} that the pure *pn* phase ends at 0.92 fm^{-3} and that the pure quark phase starts at 1.215 fm^{-3}, while the corresponding numbers for $B = 200$ MeVfm^{-3} are 1.04 and 1.57 fm^{-3}.

None of the equations of state from either the pure *pn* phase or with a mixed phase or Maxwell construction with quark degrees of freedom, result in stable configurations for densities above $\sim 10n_0$, implying thereby that none of the stars have cores with a pure quark phase. The EoS with *pn* degrees of freedom have masses $M \lesssim 2.2M_\odot$ when rotational corrections are accounted for. With the inclusion of the mixed phase, the total mass is reduced since the EoS is softer. However, there is the possibility of making very heavy quark stars for very small bag constants. For pure quark stars there is only one energy scale namely B which provides a homology transformation [29] and the maximum mass is $M_{max} = 2.0M_\odot(58\text{MeVfm}^{-3}/B)^{1/2}$ (for $\alpha_s = 0$). However, for $B \gtrsim 58$MeVfm^{-3} a nuclear matter mantle has to be added and for $B \lesssim 58$MeVfm^{-3} quark matter has lower energy per baryon than ^{56}Fe and is thus the ground state of strongly interacting matter. Unless the latter is the case, we can thus exclude the existence of such $2.2 - 2.3M_\odot$ quark stars.

In Fig. 4 we show the mass-radius relations for the various equations of state. The shaded area represents the allowed masses and radii for $\nu_{QPO} = 1060$ Hz of 4U 1820-30. Generally,

$$2GM < R < \left(\frac{GM}{4\pi^2\nu_{QPO}^2}\right)^{1/3}, \tag{14}$$

where the lower limit insures that the star is not a black hole, and the upper limit that the accreting matter orbits outside the star, $R < R_{orb}$. Furthermore, for the matter to be outside the innermost stable orbit, $R > R_{ms} = 6GM$, requires that

$$M \lesssim \frac{1 + 0.75j}{12\sqrt{6}\pi G\nu_{QPO}} \simeq 2.2M_\odot(1 + 0.75j)\frac{\text{kHz}}{\nu_{QPO}}, \tag{15}$$

where $j = 2\pi c\nu_s I/M^2$ is a dimensionless measure of the angular momentum of the star with moment of inertia I. The upper limit in Eq. (15) is the mass when ν_{QPO} corresponds to the innermost stable orbit. This is the case for 4U 1820-30 since according to [7] ν_{QPO} saturates at ~ 1060 Hz with increasing count rate.

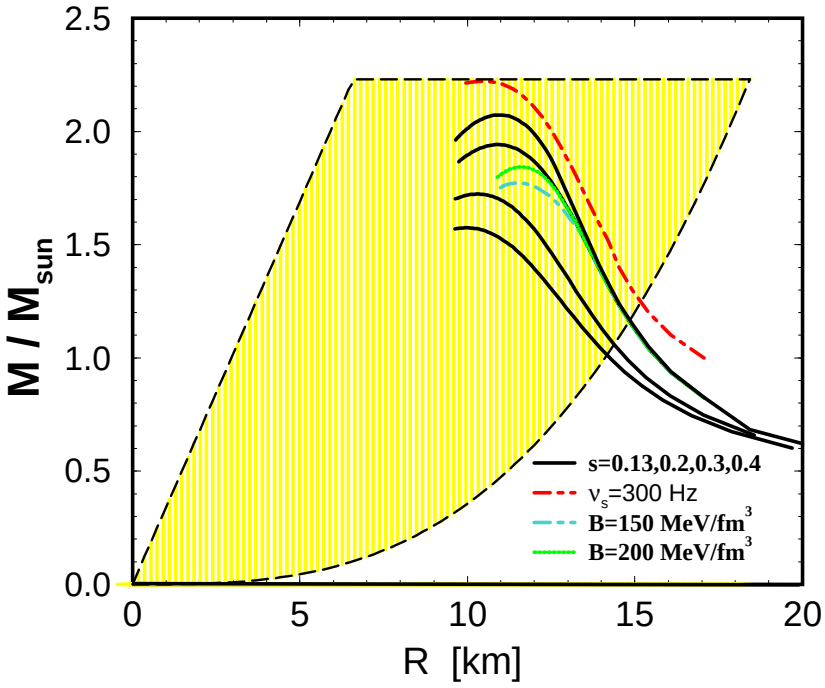

Figure 4: Neutron star masses vs. radius for the EoS of Eq. (4) with softness s=0.13,0.2,0.3,0.4, with increasing values of s from top to bottom for the full curves. Phase transitions decrease the maximum mass whereas rotation increases it. The shaded area represents the neutron star radii and masses allowed (see text and Eqs. 1-3) for orbital QPO frequencies 1060 Hz of 4U 1820-30.

The corresponding neutron star mass is $M \sim 2.2 - 2.3 M_\odot$ which leads to several interesting conclusions as seen in Fig. 4. Firstly, the stiffest EoS allowed by causality ($s \simeq 0.13 - 0.2$) is needed. Secondly, rotation must be included which increase the maximum mass and corresponding radii by 10-15% for $\nu_s \sim 300$ Hz. Thirdly, a phase transition to quark matter below densities of order $\sim 5 n_0$ can be excluded, corresponding to a restriction on the bag constant $B \gtrsim 200$ MeVfm^{-3}.

These maximum masses are smaller than those of APR98 and Kalogera & Baym who, as discussed above, obtain upper bounds on the mass of neutron stars by discontinuously setting the sound speed to equal the speed of light above a certain density, n_c. By varying the density $n_c = 2 \rightarrow 5 n_0$ the maximum mass drops from $2.9 \rightarrow 2.2 M_\odot$. In our case, incorporating causality smoothly by introducing the parameter s in Eq. (4), the EoS is softened at higher densities in order to obey causality, and yields a maximum mass lower than the $2.2 M_\odot$ derived in APR98 for nonrotating stars.

If the QPOs are not from the innermost stable orbits and one finds that even accreting neutron stars have small masses, say like the binary pulsars, $M \lesssim 1.4 M_\odot$, this may indicate that heavier neutron stars are not stable. Therefore, the EoS is soft at high densities $s \gtrsim 0.4$ or a phase transition occurs at a few times nuclear matter densities.

6 Glitches and phase transitions in rotating neutron stars

Younger pulsars rotate and slow down rapidly. Some display sudden speed ups referred to as glitches. The glitches observed in the Crab, Vela, and a few other pulsars are probably due to quakes occurring in solid structures such as the crust, superfluid vortices or possibly the quark matter lattice in the core [28]. As the rotating neutron star gradually slows down and becomes less deformed, the rigid component is strained and eventually cracks/quakes and changes its structure towards being more spherical.

The moment of inertia of the rigid component, I_c, decreases abruptly and its rotation and pulsar frequency increases due to angular momentum conservation resulting in a glitch. The observed glitches are very small $\Delta\Omega/\Omega \sim 10^{-8}$. The two components slowly relaxate to a common rotational frequency on a time scale of days (healing time) due to superfluidity of the other component (the neutron liquid). The *healing parameter* $Q = I_c/I_{tot}$ measured in glitches reveals that for the Vela and Crab pulsar about ∼3% and ∼96% of the moment of inertia is in the rigid component respectively.

If the crust were the only rigid component the Vela neutron star should be almost all crust. This would require that the Vela is a very light neutron star - much smaller than the observed ones which all are compatible with $\sim 1.4M_\odot$. If we by the lattice component include not only the solid crust but also the protons in nuclear matter (NM) (which is locked to the crust due to magnetic fields), superfluid vortices pinned to the crust and the solid QM mixed phase

$$I_c = I_{crust} + I_p + I_{sv} + I_{QM}\,, \tag{16}$$

we can better explain the large I_c for the Crab. The moment of inertia of the mixed phase is sensitive to the EoS's used. For example, for a quadratic NM EoS [28] decreasing the Bag constant from 110 to 95 MeVfm^{-3} increases I_c/I_{total} from $\sim 20\%$ to $\sim 70\%$ for a $1.4M_\odot$ neutron star - not including possible vortex pinning. The structures in the mixed phase would exhibit anisotropic elastic properties, being rigid to some shear strains but not others in much the same way as liquid crystals. Therefore the whole mixed phase might not be rigid.

As the neutron star slows down, pressures and densities increase in the center and a first order phase transition may occur. Does it leave any detectable signal at the corresponding *critical* angular velocity Ω_0 ? As described in detail in [22,1] the general relativistic equations for slowly rotating stars can be solved even with first order phase transitions since only the monopole is important. The resulting moment of inertia have the characteristic behavior for $\Omega \lesssim \Omega_0$

$$I = I_0\left(1 + c_1\Omega^2 - c_2(\Omega_0^2 - \Omega^2)^{3/2} + ...\right). \tag{17}$$

Here, c_1 and c_2 are small parameters proportional to the density difference between the two phases; however, $c_2 = 0$ for $\Omega > \Omega_0$.

In order to make contact with observation, the temporal behavior of angular velocities must be considered. The pulsars slow down at a rate given by the loss of rotational energy which one usually assumes is proportional to the rotational

angular velocity to some power (for dipole radiation $n = 3$)

$$\frac{d}{dt}\left(\frac{1}{2}I\Omega^2\right) = -C\Omega^{n+1}. \tag{18}$$

With the moment of inertia given by Eq. (17) the decreasing angular velocity can be found. The corresponding braking index depends on the second derivative $I'' = dI/d^2\Omega$ of the moment of inertia and thus diverges as Ω approaches Ω_0 from below

$$n(\Omega) \equiv \frac{\ddot{\Omega}\Omega}{\dot{\Omega}^2} \simeq n - c_1\Omega^2 + c_2\frac{\Omega^4}{\sqrt{\Omega_0^2 - \Omega^2}}\,. \tag{19}$$

The *observational* braking index $n(\Omega)$ exhibits a characteristic behavior different from the *theoretical* braking index n in case of a first order phase transition.

The critical angular velocities depend on the EoS and the critical densities. For best detection one would want the transition to occur for rapidly rotating pulsars such as millisecond pulsars, X-ray binaries or young neutron stars only a few years or centuries old. As pulsars slow down over a million years, their central densities span a wide range of order several n_0. As we are interested in time scales of years, we must instead study the ~ 1000 pulsars available. By studying the corresponding range of angular velocities for the sample of different star masses, the chance for encountering a critical angular velocity increases. Eventually, one may be able to cover the full range of central densities and find all first order phase transitions up to a certain size determined by the experimental resolution.

7 Other recent surprises related to neutron stars

7.1 Connecting NO_3^- peaks in ice core samples to supernovae

A curious connection between four NO_3^- peaks from south pole ice core samples and supernovae has recently been made. A small nearby but well hidden supernova remnant RX J0852.0-4622 was discovered [30] in the southeast corner of the older Vela supernova remnant. Estimates of its distance and age seem to be compatible with the 4th NO_3^- peak in the 20 year old south pole core samples [31]. The other three already agreed with the historical Crab, Tycho and Kepler supernovae within the ice dating accuracy of ± 20 years, a millennium back. This seems to indicate that nearby supernova explosions can affect the climate on earth and lead to geophysical signals. The radiation does produce NO_3^- in the upper atmosphere but the quantitative amount of fall out on the poles by northern/southern light cannot be estimated. NO_3^- peaks were not found in the Vostok og Greenland drills possibly because the aurorae do not have fallout on these sites. Further drillings are needed to confirm the connection - in particular deeper ones which should also include the 1006 and 1054 supernovae. Mass extinctions may be caused by nearby supernova explosions after all.

7.2 X-ray bursts and thermonuclear explosions

Slow accretion from a small mass companion $\lesssim 2M_\odot$ generates a continuous background of X-rays. Each nucleon radiates its gravitational energy of $\sim m_n GM/R \simeq$ 100 MeV. After accumulating hydrogen on the surface, pressures and temperatures become sufficient to trigger an irregular runaway thermonuclear explosion every few hours or so seen as an X-ray burst (see, e.g., [3] for a review). The energy involved is typical nuclear binding energies $\sim$ 1 MeV, i.e., a percent of the time integrated background.

The microsecond time resolution in these X-ray spectra allow for Fourier transforms in millisecond time intervals which is much shorter than the burst duration of order a few seconds. In the case of 4U 1728-34 the power analysis shows a peak at the neutron star spin frequency at 364 Hz which, however, decreases to 362 Hz during the first 1-2 seconds of the burst [9]. A simple explanation is that the thermonuclear explosion elevates the surface of the neutron star. Conserving angular momentum, $L \propto MR^2\nu$, leads to a decrease in rotation by

$$\frac{\Delta\nu}{\nu} \simeq -2\frac{\Delta R}{R}\,. \tag{20}$$

With a frequency change of $\Delta\nu \sim -2$ Hz and typical neutron star radii of order $R \sim$ 10 km, we find an elevation of order $\Delta R \sim 20$ m, which is roughly in agreement with expectations but much less than on earth due to the much stronger gravitational fields on neutron stars.

7.3 Gamma Ray Bursters and hypernovae

The recent discovery of afterglow in Gamma Ray Bursters (GRB) allows determination of the very high redshifts ($z \geq 1$) and thus the enormous distance and energy output $E \sim 10^{53}$ ergs in GRB if isotropically emitted. Very recently evidence for beaming or jets has been found [32] corresponding to "only" $E \sim 10^{51}$ ergs. Candidates for such violent events include neutron star mergers or a special class of type Ic supernova (*hypernovae*) where cores collapse to black holes. Indication of such connections are brought by recent observations of a bright supernova coinciding with GRB 980326. Binary pulsars are rapidly spiraling inwards and will eventually merge and create a gigantic explosion and perhaps collapse to a black hole. From the number of binary pulsars and spiral rates, one estimates about one merger per million year per galaxy. With $\sim 10^9$ galaxies at cosmological distances $z \lesssim 1$ this gives about the observed rate of GRB. However, detailed calculations have problems with baryon contamination, i.e. the baryons ejected absorb photons in the relativistically expanding photosphere. Accreting black holes have also been suggested to act as beaming GRB.

So far, the physics producing these GRB is not understood. The time scales and the enormous power output points towards neutron star or black hole objects.

8 Summary

Modern nucleon-nucleon potentials have reduced the uncertainties in the calculated EoS. Using the most recent realistic effective interactions for nuclear matter of APR98 with a smooth extrapolation to high densities including causality, the EoS could be constrained by a "softness" parameter s which parametrizes the unknown stiffness of the EoS at high densities. Maximum masses have subsequently been calculated for rotating neutron stars with and without first and second order phase transitions to, e.g., quark matter at high densities. The calculated bounds for maximum masses leaves two natural options when compared to the observed neutron star masses:

- **Case I**: *The large masses of the neutron stars in QPO 4U 1820-30 ($M = 2.3M_\odot$), PSR J1012+5307 ($M = 2.1 \pm 0.4M_\odot$), Vela X-1 ($M = 1.9 \pm 0.1M_\odot$), and Cygnus X-2 ($M = 1.8 \pm 0.2M_\odot$), are confirmed and complemented by other neutron stars with masses around $\sim 2M_\odot$.* The EoS of dense nuclear matter is then severely constrained and only the stiffest EoS consistent with causality are allowed, i.e., softness parameter $0.13 \leq s \lesssim 0.2$. Furthermore, any significant phase transition at densities below $< 5n_0$ can be excluded.

  That the radio binary pulsars all have masses around $1.4M_\odot$ is then probably due to the formation mechanism in supernovae where the Chandrasekhar mass for iron cores are $\sim 1.5M_\odot$. Neutron stars in binaries can subsequently acquire larger masses by accretion as X-ray binaries.

- **Case II**: *The heavy neutron stars prove erroneous by more detailed observations and only masses like those of binary pulsars are found.* If accretion does not produce neutron stars heavier than $\gtrsim 1.4M_\odot$, this indicates that heavier neutron stars simply are not stable which in turn implies a soft EoS, either $s > 0.4$ or a significant phase transition must occur already at a few times nuclear saturation densities.

Surface temperatures can be estimated from spectra and from the measured fluxes and known distances, one can extract the surface area of the emitting spot. This gives unfortunately only a lower limit on the neutron star size, R. If it becomes possible to measure both mass and radii of neutron stars, one can plot an observational (M, R) curve in Fig. (4), which uniquely determines the EoS for strongly interacting matter at low temperature.

Pulsar rotation frequencies and glitches are other promising signals that could reveal phase transitions. Besides the standard glitches also giant glitches were mentioned and in particular the characteristic behavior of angular velocities when a first order phase transition occurs right in the center of the star.

It is impossible to cover all the interesting and recent developments concerning neutron stars in these proceedings so for more details we refer to [1] and Refs. therein.

Acknowledgments

Thanks to my collaborators M. Hjorth-Jensen and C.J. Pethick as well as G. Baym, F. Lamb and V. Pandharipande.

References

1. H. Heiselberg & M. Hjorth-Jensen, 1999, *Phys. Rep.*, in press; and 1999, *Ap. J.*, in press.
2. S.E. Thorsett, & D. Chakrabarty, *Ap. J.***512** (1999) 288
3. J. van Paradijs, 1998, astro-ph/9802177 and in: The Many Faces of Neutron Stars, ed. R. Buccheri, J. van Paradijs & M. A. Alpar, in press.
4. Barziv et al., 1999, in preparation; earlier analyses (M.H. van Kerkwijk, J. van Paradijs, & E.J. Zuiderwijk, 1995, A. & A., 303, 497) have larger uncertainties.
5. J.A. Orosz, & E. Kuulkers, Mon. Not. R. Astron. Soc., 1999, in press
6. M.C. Miller, F.K. Lamb, & P. Psaltis, *Ap. J.*, 508 (1998) 791.
7. W. Zhang, T.E. Strohmayer, & J.H. Swank, 1997, *Ap. J. Lett.*, 482, L167; W. Zhang, A.P. Smale, T.E. Strohmayer, & J.H. Swank, 1998, *Ap. J. Lett.*, 500, L171
8. P. Kaaret, E.C. Ford, & K. Chen, *Ap. J. Lett.*, 480 (1997) L27
9. L. Bildsten and T. Strohmayer, *Physics Today*, feb. 1999, p. 40.
10. A. Akmal, V.R. Pandharipande, D.G. Ravenhall, *Phys. Rev.* C**58** (1998) 1804
11. V. Kalogera & G. Baym, *Ap. J. Lett.***470** (1996) L61
12. L. Engvik, M. Hjorth-Jensen, R. Machleidt, H. Müther, & A. Polls, *Nucl. Phys.* A627 (1997) 125
13. D.B. Kaplan and A.E. Nelson, *Phys. Lett.* B291 (1986) 57.
14. G. Brown, C. Lee, M. Rho and V. Thorsson, *Nucl. Phys.* **A 572** (1994) 693.
15. T. Waas, M. Rho and W. Weise, *Nucl.Phys.* **A617**, 449-463 (1997).
16. R. B. Wiringa, V. Fiks and A. Fabrocini, *Phys. Rev.* **C38** (1988) 1010.
17. V.R. Pandharipande, C.J. Pethick and V. Thorsson, *Phys. Rev. Lett.***75** (1995) 4567.
18. J. Carlson, H. Heiselberg, V.J. Pandharipande, to be published.
19. N.K. Glendenning and J. Schaffner, *Phys. Rev. Lett.***81** (1998) 4564.
20. G. Baym and C.J. Pethick, Ann. Rev. Nucl. Sci. 25 (1975) 27; Ann. Rev. Astron. Astrophys. 17 (1979) 415.
21. A.B. Migdal, E.E. Saperstein, M.A. Troitsky and D.N. Voskresensky, *Phys. Rep.***192** (1990) 179.
22. H. Heiselberg & M. Hjorth-Jensen, *Phys. Rev. Lett.***80** (1998) 5485.
23. C.P. Lorenz, D.G. Ravenhall, C.J. Pethick, *Phys. Rev. Lett.***70** (1993) 379
24. B. deMarco and D.S. Jin, *cond-mat/9807406*, and *Science*, sept. 10., 1999.
25. L.P. Gorkov & T.K. Melik-Barkhudarov, JETP **13** (1961) 1018.
26. J. P. Blaizot, J. F. Berger, J. Decharge, & M. Girod, *Nucl. Phys.* A**591** (1995) 435
27. N.K. Glendenning, *Phys. Rev.* D**46** (1992) 1274
28. H. Heiselberg, C.J. Pethick, & E.F. Staubo, *Phys. Rev. Lett.***70** (1993) 1355
29. J. Madsen, preprint astro-ph/9809032.
30. B. Aschenbach, *Nature* 396, 141 (1998).
31. R.T. Rood, C.L. Sarazin, E.J. Zeller and B.C. Parker, *Nature* 282, 701 (1979).
32. S.R. Kulkarni et al., astro-ph/9905301+6.